



Analysis of Different Levels of Approximation of the Reynolds Stress Tensor for a Boundary Layer Flow

Angela O. Nieckele

Department of Mechanical Engineering, PUC-Rio
Rua Marques de São Vicente 225, Gávea, 22453-900, Rio de Janeiro, RJ, Brazil
nieckele@puc-rio.br

Roney Leon Thompson

LMTA-PGMEC, Department of Mechanical Engineering, Fluminense Federal University
Rua Passo da Pátria 156, São Domingos, 24210-240, Niterói, RJ, Brazil
rthompson@mec.uff.br

Gilmar Mompean

University of Lille Nord de France, Polytech'Lille, F-59000 Lille,
LML, CNRS UMR 8107, F-59655 Villeneuve d'Ascq, France
gilmar.mompean@polytech-lille.fr

Abstract. *In order to solve the average velocity field in the Reynolds Average Navier Stokes approach, closure equations that relate the Reynolds stress tensor to the mean kinematic tensors are necessary. While the Boussinesq hypothesis assume a linear relation between the Reynolds stress tensor, R , and the rate-of-strain tensor, D , other hypothesis can be tested. In particular the relative vorticity, W^* , the vorticity computed with respect to the rate of rotation of the eigenvectors of D , is an objective tensor that can play an important role on a number of turbulent flows. It can be shown that the ability of the fluid to avoid been stretched by the flow is related to a high intensity of the non-persistence-of-straining tensor, DW^*-W^*D . Based on this tensor and on D , different sets of basis tensors can be used in order to express the Reynolds stress tensor. In the present methodology, experimental results of the turbulent boundary layer flow are used to compute R , D , and DW^*-W^*D and by decomposition tensor theorems, the coefficients of a variety of models are computed and indices that indicate the degree of agreement between the different models and the Reynolds stress tensor are calculated. Depending on the chosen model, different regions of the flow are better captured and an analysis associating the tensor basis and the prediction capacity is provided.*

Keywords: *boundary layer, RANS, tensor decomposition, turbulent closures*

1. INTRODUCTION

Numerical simulations of turbulent flows have become a valuable tool to predict the behavior of such flows, not only for problems of scientific interest, but also it has been largely applied for several engineering applications. This applications concerns different fields with industrial and practical applications: aeronautics and automotive engineering, meteorology, environment, etc.

Attempts to predict the turbulent characteristics have been made with different computational approaches, which can generally be classified as Direct Numerical Simulation (DNS), Large Eddy Simulation (LES) or Reynolds Averaged Navier–Stokes (RANS). Direct Numerical Simulation resolves the full 3D transient Navier–Stokes equations, without introducing any modeling, therefore, a very fine mesh and time step is required. The results from the DNS are very accurate and reveal valuable information on the turbulence structures and are very useful to develop second-order turbulence models. However, the DNS approach is limited to low Reynolds numbers. An alternative to the DNS approach is the technique of LES. The LES approach is a numerical technique used to solve the partial differential equations governing turbulent fluid flow. The idea is to solve directly the large scales which are responsible for carrying most of the flow energy and to model the small scales within the mesh size, where the energy is dissipated. Therefore, the LES approach requires a sub-grid model. Although 3D transient Navier–Stokes equations are solved, the mesh size, as well as the time step, does not need to be as small as with the DNS methodology, resulting in less computational effort, but more effort than those methods that solve the Reynolds-averaged Navier–Stokes equations (RANS). The RANS approach requires the derivation of modeled equations from the instantaneous Navier–Stokes equations using the Reynolds decomposition. Reynolds decomposition refers to separation of the flow variable into the mean component and the fluctuating component. As a consequence of the average process, additional terms named as turbulent Reynolds Stress appear on the equations and need to be modeled. When using this approach, the success of computational results depends heavily on the choice of the Reynolds Stress Models. In this study, Explicit Algebraic Reynolds Stress Models (EARSMS) is used. These EARSMS models propose the relations between Reynolds stress tensor, mean rate of deformation and the vorticity tensors, and they are able to capture more characteristics of the turbulent flows (anisotropy, near-wall behavior).

A.O. Nieckele, Thompson, R.L., Mompean, G.

Analysis of different levels of approximation of the Reynolds stress tensor for a boundary layer flow

There are two ways to evaluate RANS turbulence models: a) use the model in a Navier–Stokes solver (a posteriori test) or use mean fields evaluated from DNS or from experimental data in the model and compare with the Reynolds stress computed with DNS or with the measured values (a priori test), see e.g. Mompean et al. (1996); Naji et al. (2004), Schmitt (2007). One of the most widespread closure assumptions used in turbulence modeling is that of an eddy viscosity linking the deviatoric Reynolds stresses tensor linearly to the local mean strain. This type of closure is known to be incapable of predicting some well-established turbulent phenomena such as the effects of streamline curvature, rotation, and turbulence induced secondary flows near corners.

The focus of this paper is to present a methodology to evaluate the Reynolds stress dependence upon mean kinematic tensors. The proposed methodology is based upon tensor decomposition theorems that allow determination of the orientation of the Reynolds stress tensor from the experimental data of boundary layer flows. The prediction of the turbulent boundary layer is important for several practical applications, aircrafts, ships, submarines and offshore platforms. In this work, experimental data of turbulent boundary layers from Carlier and Stanislas (2005), Stanislas et al. (2008) are used. In these works the authors presented a study concerning the identification of vertical structures in the turbulent boundary layer. Coherent structures corresponding to hairpin vortex are analyzed through stereoscopic particle image velocimetry. Measurements using hot-wire anemometers were also made in the boundary layer and is used in this work. Through comparisons using these experimental boundary layer databases, the methodology presented below allows to quantify how good the tensorial formulation of the Reynolds stress tensor is, and compute the scalar coefficients appearing in the six models tested in this work. Using this methodology, it is shown in this paper the improvement of the modeling to produce accurate RANS turbulent models.

The outline of the paper is as follows. Section 2 presents the methodology based upon tensor decomposition theorem. The results are presented in section 3. Conclusions are drawn in section 4.

2. METHODOLOGY

The following usual Reynolds decomposition notations will be used: $(\bar{\quad})$ indicates the time average operation and a single quote (') denotes the fluctuations with respect to the average. The Reynolds stress tensor, \mathbf{R} , is defined through

$$\mathbf{R} = -\overline{\mathbf{u}'\mathbf{u}'} \quad (1)$$

and the traceless Reynolds stress tensor \mathbf{a} is defined as

$$\mathbf{a} = \mathbf{R} - \frac{1}{3} \text{tr}(\mathbf{R}), \quad (2)$$

where $\text{tr}(\cdot)$ is the trace operator.

2.1 Tensor decompositions

Two kinds of decompositions of a tensor with respect to a second one have been employed. These two kinds were shown by Thompson et al. (2010) to be the only ones that decouple the tensor into a part which is coaxial and another which is orthogonal to the second one and at the same time these two parts of the decomposition are orthogonal to each other. One decomposition is referred to as proportional-orthogonal and the other one in-phase-out-of-phase decompositions. The proportional-orthogonal decomposition of a tensor \mathbf{U} with respect to a tensor \mathbf{V} is given by

$$\mathbf{U} = \frac{\text{tr}(\mathbf{U} \cdot \mathbf{V})}{\text{tr}(\mathbf{V} \cdot \mathbf{V})} \mathbf{V} + \frac{\text{tr}(\mathbf{V} \cdot \mathbf{V})\mathbf{U} - \text{tr}(\mathbf{U} \cdot \mathbf{V})\mathbf{V}}{\text{tr}(\mathbf{V} \cdot \mathbf{V})} \quad (3)$$

where the first term on the r.h.s of Eq. (3) is proportional to \mathbf{V} , while the second one is orthogonal to \mathbf{V} . The in-phase-out-of-phase decomposition is given by

$$\mathbf{U} = \mathbf{1}\mathbf{V}\mathbf{V} : \mathbf{U} + (\mathbf{1}\delta\delta - \mathbf{1}\mathbf{V}\mathbf{V}) : \mathbf{U} \quad (4)$$

where the fourth order tensors that appear in Eq. (4) are given by

$$\mathbf{1}\mathbf{V}\mathbf{V} = \sum_{i=1}^3 \mathbf{e}_i^{\mathbf{V}} \otimes \mathbf{e}_i^{\mathbf{V}} \otimes \mathbf{e}_i^{\mathbf{V}} \otimes \mathbf{e}_i^{\mathbf{V}} \quad (5)$$

where the unit vectors are eigenvectors of \mathbf{V} and

$$\mathbf{1}^{\otimes 4} = \mathbf{e}_p \otimes \mathbf{e}_q \otimes \mathbf{e}_q \otimes \mathbf{e}_p \quad (6)$$

where the Einstein convention is assumed. The mathematical analysis of these decompositions is discussed in Thompson (2008).

These two tensor decompositions were applied to the Reynolds stress tensor with respect to two kinematic tensors: the symmetric part of the velocity gradient, \mathbf{D} and the non-persistence-of-straining tensor \mathbf{P} , defined by

$$\mathbf{P} = \mathbf{D} \mathbf{W}^* - \mathbf{W}^* \mathbf{D} \quad (7)$$

where \mathbf{W}^* is the relative vorticity tensor, defined as the vorticity measured with respect to the rate of rotation of the eigenvectors of \mathbf{D} . Since \mathbf{D} and \mathbf{P} are orthogonal, it is possible to produce 6 levels of representations of the Reynolds stress, depending on the combinations of the decompositions adopted. Besides that, indices of adherence to quantify the ability of the particular model to capture the Reynolds tensor were applied.

2.2 The models

The six models presented in the present work are

$$M_I : \mathbf{a}_I = \alpha \mathbf{D} \quad (8)$$

$$M_{II} : \mathbf{a}_{II} = \alpha_o \mathbf{I} + \alpha_D \mathbf{D} + \alpha_{D2} \mathbf{D}^2 \quad (9)$$

$$M_{III} : \mathbf{a}_{III} = \alpha_o \mathbf{I} + \alpha_D \mathbf{D} + \alpha_{D2} \mathbf{D}^2 + \beta_P \mathbf{P} \quad (10)$$

$$M_{IV} : \mathbf{a}_{IV} = \alpha_D \mathbf{D} + \beta_P \mathbf{P} \quad (11)$$

$$M_V : \mathbf{a}_V = \beta_o \mathbf{I} + \alpha_D \mathbf{D} + \beta_P \mathbf{P} + \beta_{P2} \mathbf{P}^2 \quad (12)$$

$$M_{VI} : \mathbf{a}_{VI} = (\alpha_o + \beta_o) \mathbf{I} + \alpha_D \mathbf{D} + \alpha_{D2} \mathbf{D}^2 + \beta_P \mathbf{P} + \beta_{P2} \mathbf{P}^2 \quad (13)$$

and the indexes, Idx_i ; $i \in \{I; II; III; IV; V; VI\}$ that measure the quality of the approximations are given by

$$Idx_i = 1 - \frac{2}{\pi} \cos^{-1} \sqrt{\frac{\text{tra}_i^2}{\text{tra}^2}} \quad (14)$$

where \mathbf{a} is the anisotropy Reynolds stress tensor calculated from the experiments.

The quantities Idx_i ; are local. It is straightforward to infer that, at any point of the domain, the following inequalities hold:

$$0 \leq Idx_I \leq Idx_{II} \leq Idx_{III} \leq Idx_{VI} \leq 1 \quad (15)$$

$$0 \leq Idx_I \leq Idx_{IV} \leq Idx_V \leq Idx_{VI} \leq 1 \quad (16)$$

$$0 \leq Idx_I \leq Idx_{IV} \leq Idx_{III} \leq Idx_{VI} \leq 1 \quad (17)$$

From the inequalities above, it can be established the different complexity levels of approximation. One important issue is to address the differences between models of the same level of complexity such as the pair M_{II} and M_{IV} and the pair M_{III} and M_V .

3. RESULTS AND DISCUSSION

The models described in the previous section were applied to the experimental data of a boundary layer flow (Carlier and Stanislas, 2005, Stanislas et al., 2008). The friction velocity u_τ is measured directly by PIV very near to the wall, with an accuracy which is of the order of 1%. Hot wire probe was employed to measure the mean flow velocity U and the standard deviation $\sqrt{u^2}$. The Reynolds stress \overline{uv} and standard deviations $\sqrt{v^2}$ and $\sqrt{w^2}$ were measured with cross wires probe. The axial, normal and transversal velocity components were measured at different normal x_2 positions. Their values were interpolated to the same position in order to allow the determination of the Reynolds stress tensor corresponding to each model.

A.O. Nieckele, Thompson, R.L., Mompean, G.
 Analysis of different levels of approximation of the Reynolds stress tensor for a boundary layer flow

The momentum Reynolds number Re_θ is based on the external velocity U_∞ and the momentum thickness θ , while the frictional Reynolds number is based on boundary layer thickness δ and friction velocity u_τ ,

$$Re_\theta = U_\infty \theta / \nu \quad ; \quad Re_\tau = u_\tau \delta / \nu \tag{18}$$

where $\nu = \mu/\rho$ is the kinematic viscosity, ρ is the density and μ the molecular viscosity.

Four cases were considered to evaluate the tensor decomposition technique. Table 1 presents the corresponding Reynolds numbers.

Table 1. Test Cases

Case	1	2	3	4
Re_θ	8171	11454	14505	20831
Re_τ	2680	3891	4941	7164

Figure 1 illustrates the measured velocities variation along the dimensionless wall distance $y^+ = u_\tau y / \nu$, corresponding to $Re_\tau = 2680$. The velocities were normalized with the friction velocity u_τ .

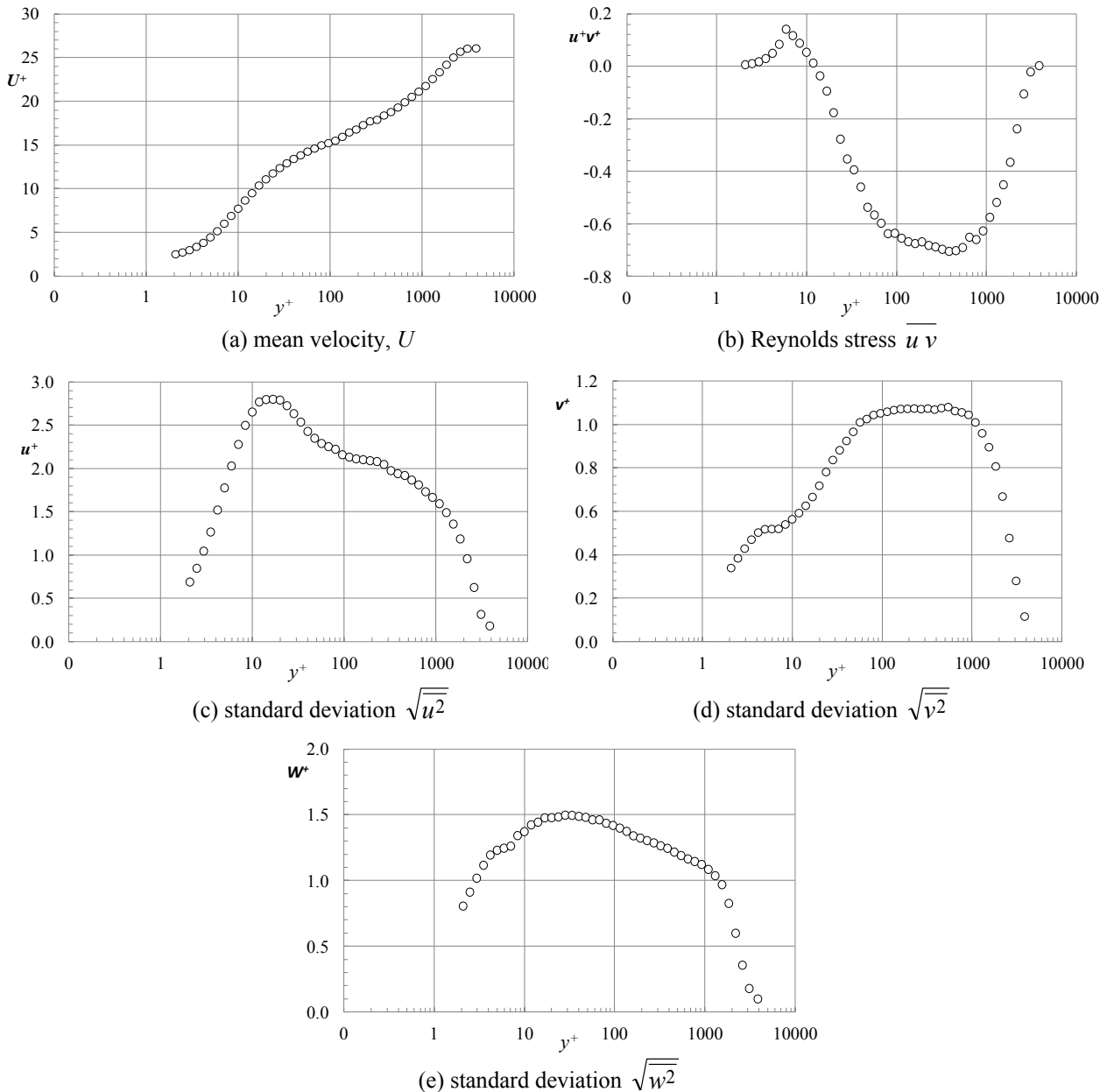


Figure 1. Experimental velocities, $Re_\tau=2680$.

Figure 1a corresponds to the mean axial velocity, while Fig. 1b shows the Reynolds stress. The standard deviation in the x , y and z directions are shown in Figs. 1c, 1d and 1e, respectively. From these data, the mean kinematic tensors corresponding to the different models presented in the previous section were determined, and the normalized index of each model was evaluated.

Figures 2 and 3 present a comparison of the dimensionless traceless Reynolds stress tensor, obtained with each model, with the experimental data, for the smallest and highest Reynolds number investigated. The traceless Reynolds stress tensor is defined as $\mathbf{a}^+ = \mathbf{a}/u_{\tau}^2$ where $\mathbf{a} = \mathbf{R} - (1/3) \text{tr}(\mathbf{R})$. Note that, as already mentioned, the Reynolds number does not influence the behavior of the dimensionless Reynolds stress.

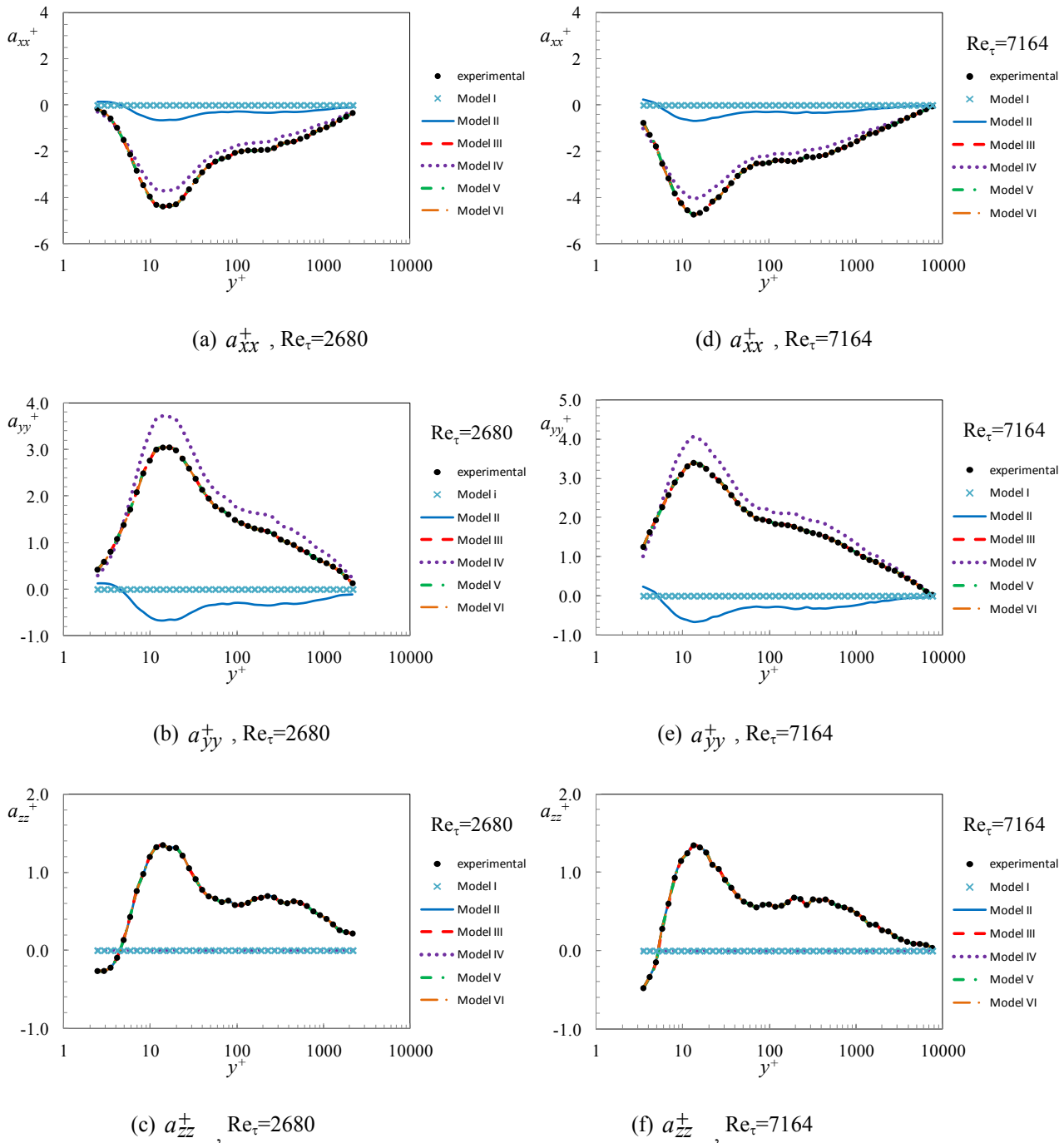


Figure 2. Components of the traceless Reynolds stress tensor. $Re_{\tau}=2680$ and $Re_{\tau}=7164$.

Analyzing Fig. 2, it can be seen that Model I cannot predict the normal contribution of the Reynolds stress. Model II predicts the same distribution for a_{xx}^+ and a_{yy}^+ , and fails to predict a_{zz}^+ . Models III, V and VI are able to obtain for the

A.O. Nieckele, Thompson, R.L., Mompean, G.

Analysis of different levels of approximation of the Reynolds stress tensor for a boundary layer flow

three normal components of the traceless Reynolds stress, with exactly the same distribution as measured tensor. Although Model IV predicts quite well a_{xx}^+ and a_{yy}^+ , it fails to predict a_{zz}^+ . The shear stress contribution is shown in Fig. 3 for both Reynolds numbers and all models. As expected, for this kind of simple flow, all models present an excellent result for a_{xy}^+ , with perfect agreement with the experimental data.

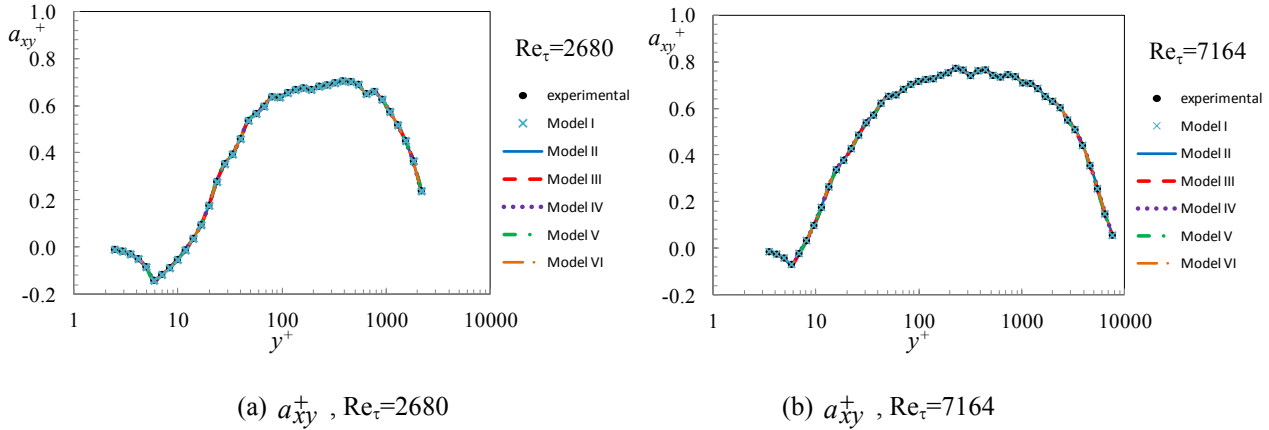


Figure 3. Components of the traceless Reynolds stress tensor. $Re_\tau=2680$ and $Re_\tau=7164$.

To help analyze the results, it should be noted that, with the available experimental data, the symmetric part of the velocity gradient \mathbf{D} and the Reynolds stress tensor \mathbf{R} have the following form

$$D = \begin{pmatrix} 0 & D_{12} & 0 \\ D_{12} & 0 & 0 \\ 0 & 0 & 0 \end{pmatrix} ; \quad R = \begin{pmatrix} R_{11} & R_{12} & 0 \\ R_{12} & R_{22} & 0 \\ 0 & 0 & R_{33} \end{pmatrix} \quad (19)$$

The traceless Reynolds stress tensor corresponding to each model is

$$M_I = \begin{pmatrix} 0 & M_{I12} & 0 \\ M_{I12} & 0 & 0 \\ 0 & 0 & 0 \end{pmatrix} ; \quad M_{II} = \begin{pmatrix} M_{II11} & M_{II12} & 0 \\ M_{II12} & M_{II11} & 0 \\ 0 & 0 & M_{II33} \end{pmatrix} \quad (20)$$

$$M_{IV} = \begin{pmatrix} M_{IV11} & M_{IV12} & 0 \\ M_{IV12} & -M_{IV11} & 0 \\ 0 & 0 & 0 \end{pmatrix} ; \quad M_k = \begin{pmatrix} M_{k11} & M_{k12} & 0 \\ M_{k12} & M_{k22} & 0 \\ 0 & 0 & M_{k33} \end{pmatrix} ; \quad k = \text{III, V and VI} \quad (21)$$

The correlation coefficient regarding the six models is presented in Fig. 4 for all Reynolds numbers. Note that the correlation index is equal to one for models III, V and VI. Examining Fig. 4a, it can be seen that the Reynolds number does not affect the correlation index, since similar results were obtained for all Reynolds numbers. The smallest correlation index corresponds to model I, followed by model II. Both models present similar behavior, with an increase of the index as y^+ increases. Model IV presents an approximately constant correlation index, along the boundary layer, approximately equal to 0.8.

Comparing the traceless Reynolds stress tensor of each model (M_k , $k=I \dots VI$) with the Reynolds stress \mathbf{R} , it is clear that all models are able to capture the shear component. Model I cannot capture the normal contribution and Model II is not able to capture the flow anisotropy, since $a_{xx}^+ = a_{yy}^+$ and a_{zz}^+ is zero. This explains why their correlation index is low. The index increases away from the wall, because the stress contribution diminishes in that direction. The correlation index of Model IV is high (≈ 0.8), because it can also predict reasonable well a_{xx}^+ and a_{yy}^+ . The failure to predict a_{zz}^+ is reflected in the reduction of the correlation index. Models III, V and VI can predict all traceless Reynolds

stress components, and the correlation index is equal to one throughout the whole boundary layer. These results indicate the importance of considering the non-persistence-of-straining tensor \mathbf{P} in the models.

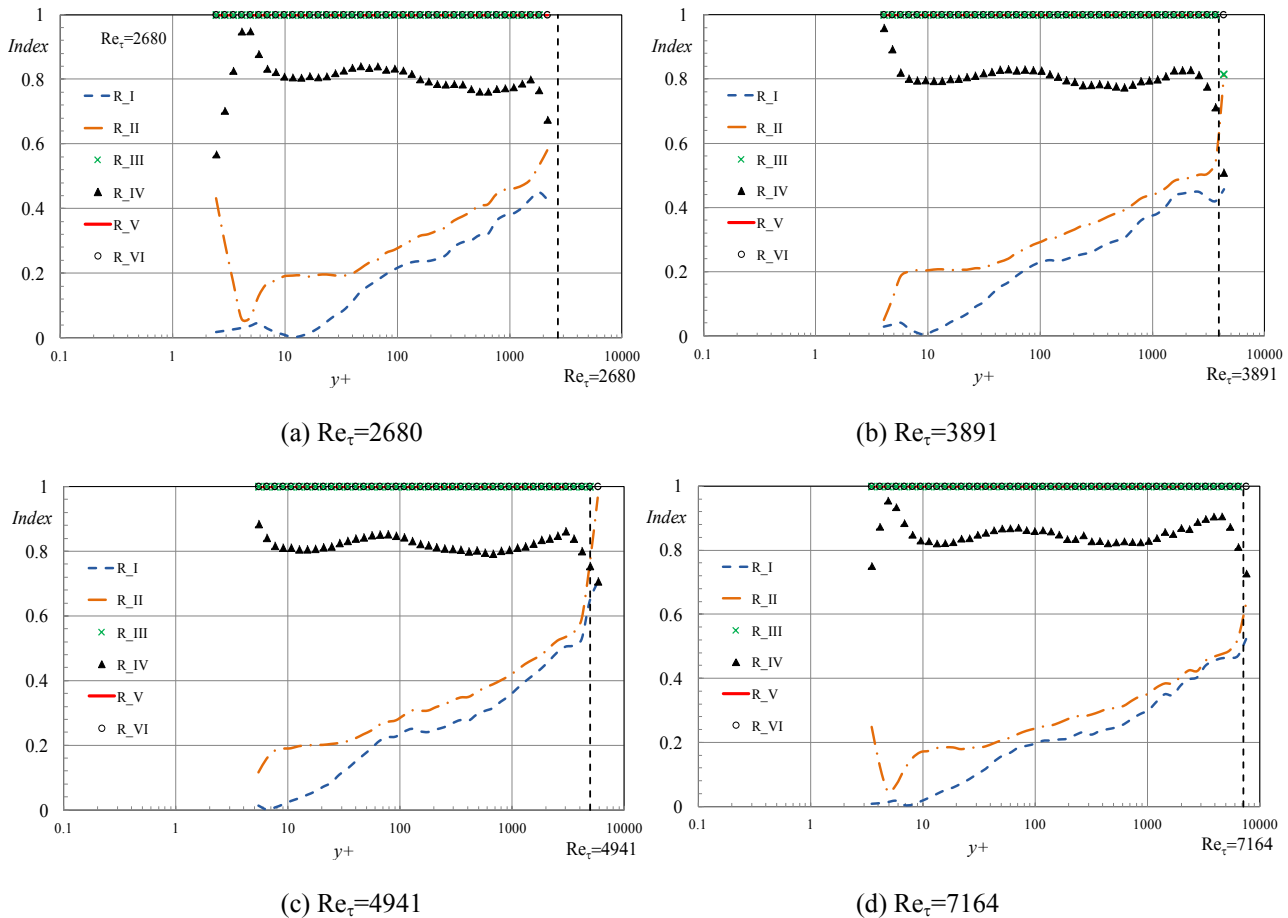


Figure 4. Index of several models. $Re_\tau=2680$, $Re_\tau=3891$, $Re_\tau=4941$ and $Re_\tau=7164$

4. CONCLUSION

Six different models for representing the anisotropic Reynolds stress tensor were presented. They are based on linear and non-linear descriptions as functions of the rate of strain and persistence of straining tensors. The use of the rate of strain tensor is customary in the literature. There are examples of using the non-objective version of the persistence of straining tensor, with the vorticity in the place of relative-vorticity tensor. These tensors have the property of being orthogonal to the rate of strain tensor and, therefore, are able to explain parts of the Reynolds stress tensor which are impossible for the rate of strain.

Experimental data of a boundary layer flow were employed to determine the Reynolds stress according to the six models and correlation index were calculated to allow evaluation of their performance. All models were able to determine accurately the shear stress. Models III, V and VI showed a superior performance, being able to represent correctly all traceless Reynolds stress components. The correlation index of Models I and II were low, since these models cannot capture flow anisotropy. For this type of flow, Model IV was able to predict reasonable traceless Reynolds stress.

The results of the present work can be useful to build models for the Reynolds stress tensor, by constructing the dependence of the coefficients as functions of the relevant parameters.

5. ACKNOWLEDGEMENTS

The authors thank Jean-Marc Foucaut and Michel Stanislas for providing the data to the development of this work. The first two authors would also wish to thank CNPq for the continuous support.

A.O. Nieckele, Thompson, R.L., Mompean, G.
 Analysis of different levels of approximation of the Reynolds stress tensor for a boundary layer flow

6. REFERENCES

- Carlier, J., Stanislas, M., 2005. "Experimental study of eddy structures in a turbulent boundary layer using particle image velocimetry." *Journal of Fluid Mechanics*, Vol. 535, p. 143-188.
- Mompean, G., Gavrilakis, S. Machiels, L. and Deville, M., 1996. "On predicting the turbulence induced secondary flows using non-linear $k - \epsilon$ models", *Physics of Fluids*, Vol. 8, p. 1856-1868.
- Naji, H., Mompean, G. and El Yahyaoui, O., 2004. Evaluation of explicit algebraic stress models using direct numerical simulations, *Journal of Turbulence*, Vol. 5 (038), p. 1-25.
- Schmitt, F. G., 2007, Direct test of nonlinear constitutive equation for simple turbulent shear flows using DNS data, *Communication in Nonlinear Science and Numerical Simulation.*, Vol. 12, p. 1251-1264.
- Stanislas, M., Perret, L., Foucaut, J., 2008. "Vortical structures in the turbulent boundary layer: a possible route to a universal representation." *Journal of Fluid Mechanics*, Vol. 602, p. 327-382.
- Thompson, R.L., 2008. "Some perspectives on the dynamic history of a material element". *International Journal of Engineering Science*, Vol. 46, p. 524-549.
- Thompson, R.L., Mompean, G. and Thais, L., 2010. "A methodology to quantify the non-linearity of the Reynolds stress tensor." *Journal of Turbulence*, Vol. 11, p. 1-27.

7. RESPONSIBILITY NOTICE

The authors are the only responsible for the printed material included in this paper.